Promises and Challenges of Metabolic Imaging: Where Does ^{18}F-FDG Stand in the Immunometabolism Era?

Sina Tavakoli

Department of Radiology, University of Pittsburgh, and Heart, Lung, Blood, and Vascular Medicine Institute, UPMC Department of Medicine, Pittsburgh, Pennsylvania

Since its development in the late 1970s, ^{18}F-FDG has been a major driver of basic science and translational discoveries, which have revolutionized the day-to-day clinical practice of nuclear imaging (*1*). Initially launched as a tracer for imaging brain metabolism, ^{18}F-FDG rapidly found its major applications in oncologic imaging through detection of cancer-associated enhanced glucose utilization and aerobic glycolysis, referred to as the Warburg effect (*1*). ^{18}F-FDG PET is now an inseparable imaging modality for the diagnosis, staging, and monitoring of therapeutic response for a variety of cancers. Beyond oncology, ^{18}F-FDG PET has been widely used in a multitude of infectious and inflammatory diseases, including sarcoidosis and vasculitis (*2*). Despite this widespread clinical use, the biologic basis of ^{18}F-FDG uptake in inflammation has been an evolving concept for nearly 3 decades.

The paper by Kubota et al. in this anniversary issue of *JNM* was a landmark study highlighting the significance of ^{18}F-FDG uptake by tumor macrophages in a mouse xenograft model during the initial years of ^{18}F-FDG biologic validation (*3*). This study extended the existing knowledge about the accumulation of ^{18}F-FDG in abscesses and other inflamed tissues by elegantly demonstrating that immune cells, and notably macrophages, are a major contributor of ^{18}F-FDG uptake in tumors (*3*). Through a series of meticulous dual-isotope (^{14}C and ^{18}F) high-resolution autoradiography images, the authors demonstrated that macrophages surrounding the necrotic part of tumors and the inflammatory granulation tissue in the periphery of tumors have a markedly higher uptake of ^{18}F-FDG than do malignant tumor cells (*3*).

Received Jun. 16, 2020; revision accepted Jun. 18, 2020.
For correspondence or reprints contact: Sina Tavakoli, UPMC Presbyterian Hospital, 200 Lothrop St., Suite E200, Pittsburgh, PA 15213.
E-mail: sit23@pitt.edu

DOI: 10.2967/jnumed.120.251744

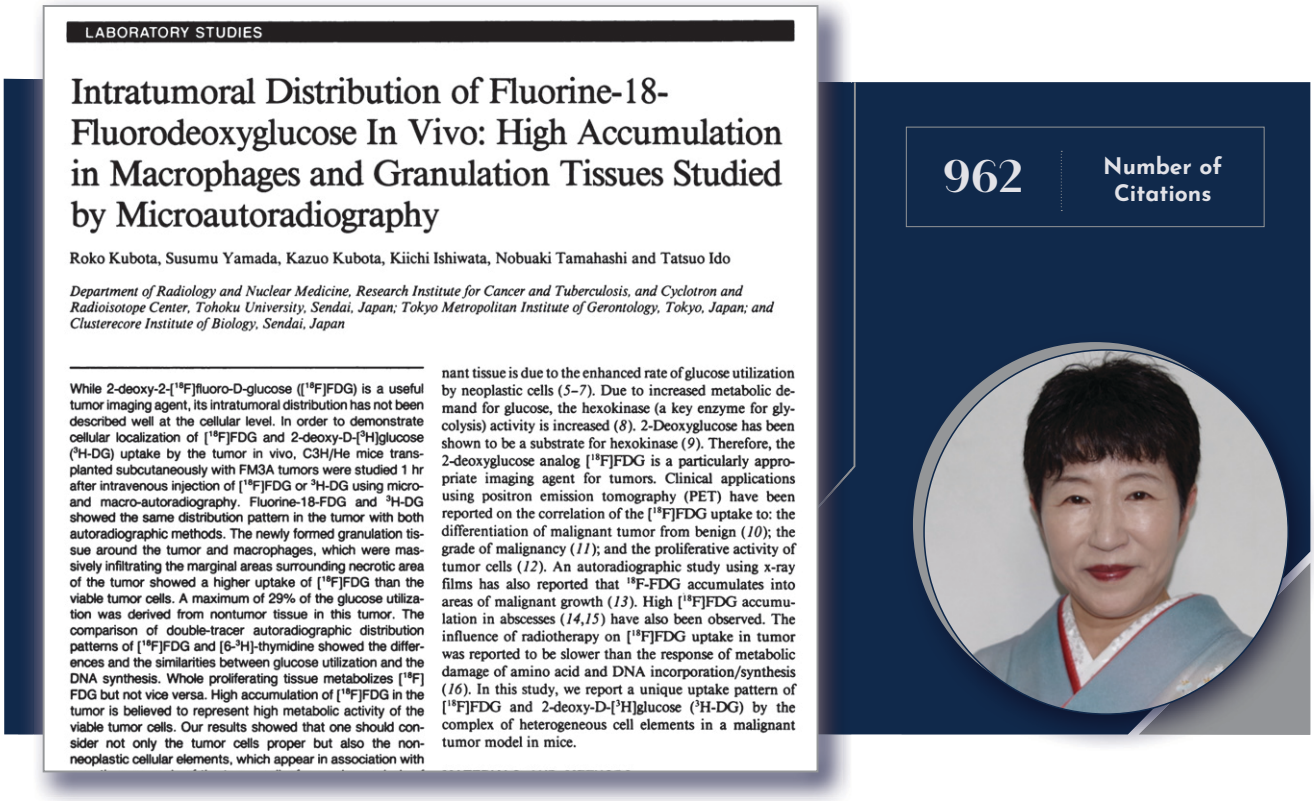

After nearly 3 decades, it is now well recognized that tumor-associated macrophages may constitute a large fraction of tumor mass and are critical players throughout different stages of tumorigenesis, from cancer initiation to local spread and metastasis (*4*). Moreover, growing immunometabolic discoveries have highlighted the cross talk between cell metabolism and macrophage biology, which may be exploited as novel targets for cancer diagnosis, risk stratification, and therapy (*4*). However, the field of immunometabolism has been driven largely through ex vivo techniques, such as stable isotope metabolic tracing, which do not accurately reflect the complexities of the natural microenvironment of tumor or inflammatory tissues.

Metabolic imaging is well positioned to address the dire need to define metabolism in vivo. However, major challenges are yet to be overcome, particularly for metabolic assessment of complex and heterogeneous tissues, such as tumors. The spatial resolution of PET does not allow ^{18}F-FDG uptake by malignant cells to be distinguished from uptake by tumor-associated macrophages or other tumor constituents. Therefore, unraveling the biologic significance of ^{18}F-FDG uptake by tumor-associated macrophages and its implications for prognostication of patients (e.g., determining tumor aggressiveness) and monitoring the response to therapy remain an ongoing challenge. Complementing in vivo PET studies by high-resolution microautoradiography (as in Kubota et al. (*3*)) or state-of-the-art metabolomics techniques (e.g., mass spectrometry imaging (*5*)) advances our knowledge about the heterogeneity of immune cell metabolism within the tumor microenvironment. The limited specificity of ^{18}F-FDG, which targets a nearly ubiquitous metabolic process, is another major challenge for the elucidation of immunometabolic links between tumor-associated macrophages and tumor biology by in vivo imaging.

A multipronged approach that includes developing novel tracers with more specific metabolic targets, imaging additional pathways other than glucose uptake, and improving the spatial resolution of PET (e.g., by total-body acquisition), along with careful histologic validations, will be vital to reinforce the role of in vivo imaging in understanding immunometabolism.

DISCLOSURE

The author is supported by the National Institutes of Health (NHLBI K08-HL144911). No other potential conflict of interest relevant to this article was reported.

REFERENCES

1. Alavi A, Reivich M. Guest editorial: the conception of FDG-PET imaging. *Semin Nucl Med*. 2002;32:2–5.
2. Jamar F, Buscombe J, Chiti A, et al. EANM/SNMMI guideline for ^{18}F-FDG use in inflammation and infection. *J Nucl Med*. 2013;54:647–658.
3. Kubota R, Yamada S, Kubota K, Ishiwata K, Tamahashi N, Ido T. Intratumoral distribution of fluorine-18-fluorodeoxyglucose in vivo: high accumulation in macrophages and granulation tissues studied by microautoradiography. *J Nucl Med*. 1992;33:1972–1980.
4. O'Sullivan D, Sanin DE, Pearce EJ, Pearce EL. Metabolic interventions in the immune response to cancer. *Nat Rev Immunol*. 2019;19:324–335.
5. Aichler M, Walch A. MALDI imaging mass spectrometry: current frontiers and perspectives in pathology research and practice. *Lab Invest*. 2015;95:422–431.

Intratumoral Distribution of Fluorine-18-Fluorodeoxyglucose In Vivo: High Accumulation in Macrophages and Granulation Tissues Studied by Microautoradiography

Roko Kubota, Susumu Yamada, Kazuo Kubota, Kiichi Ishiwata, Nobuaki Tamahashi, and Tatsuo Ido

Department of Radiology and Nuclear Medicine, Research Institute for Cancer and Tuberculosis, and Cyclotron and Radioisotope Center, Tohoku University, Sendai, Japan; Tokyo Metropolitan Institute of Gerontology, Tokyo, Japan; and Clusterecore Institute of Biology, Sendai, Japan

While 2-deoxy-2-[^{18}F]fluoro-D-glucose ([^{18}F]FDG) is a useful tumor imaging agent, its intratumoral distribution has not been described well at the cellular level. In order to demonstrate cellular localization of [^{18}F]FDG and 2-deoxy-D-[^{3}H]glucose (^{3}H-DG) uptake by the tumor in vivo, C3H/He mice transplanted subcutaneously with FM3A tumors were studied 1 hr after intravenous injection of [^{18}F]FDG or ^{3}H-DG using micro- and macro-autoradiography. Fluorine-18-FDG and ^{3}H-DG showed the same distribution pattern in the tumor with both autoradiographic methods. The newly formed granulation tissue around the tumor and macrophages, which were massively infiltrating the marginal areas surrounding necrotic area of the tumor showed a higher uptake of [^{18}F]FDG than the viable tumor cells. A maximum of 29% of the glucose utilization was derived from nontumor tissue in this tumor. The comparison of double-tracer autoradiographic distribution patterns of [^{18}F]FDG and [6-^{3}H]-thymidine showed the differences and the similarities between glucose utilization and the DNA synthesis. Whole proliferating tissue metabolizes [^{18}F]FDG but not vice versa. High accumulation of [^{18}F]FDG in the tumor is believed to represent high metabolic activity of the viable tumor cells. Our results showed that one should consider not only the tumor cells proper but also the nonneoplastic cellular elements, which appear in association with growth or necrosis of the tumor cells, for precise analysis of [^{18}F]FDG uptake in tumor-bearing subjects, especially after anti-neoplastic treatment.

J Nucl Med 1992; 33:1972–1980
DOI: 10.2967/jnumed.120.251744a

Fluorine-18-2-deoxy-2-glucose ([^{18}F]FDG) has been shown to be a useful tumor-detecting agent (*1–4*). The mechanism of accumulation of this tracer into the malignant tissue is due to the enhanced rate of glucose utilization by neoplastic cells (*5–7*). Due to increased metabolic demand for glucose, the hexokinase (a key enzyme for glycolysis) activity is increased (*8*). 2-Deoxyglucose has been shown to be a substrate for hexokinase (*9*). Therefore, the 2-deoxyglucose analog [^{18}F]FDG is a particularly appropriate imaging agent for tumors. Clinical applications using positron emission tomography (PET) have been reported on the correlation of the [^{18}F]FDG uptake to: the differentiation of malignant tumor from benign (*10*); the grade of malignancy (*11*); and the proliferative activity of tumor cells (*12*). An autoradiographic study using x-ray films has also reported that ^{18}F-FDG accumulates into areas of malignant growth (*13*). High [^{18}F]FDG accumulation in abscesses (*14,15*) have also been observed. The influence of radiotherapy on [^{18}F]FDG uptake in tumor was reported to be slower than the response of metabolic damage of amino acid and DNA incorporation/synthesis (*16*). In this study, we report a unique uptake pattern of [^{18}F]FDG and 2-deoxy-D-[^{3}H]glucose (^{3}H-DG) by the complex of heterogeneous cell elements in a malignant tumor model in mice.

MATERIALS AND METHODS

Animal Model

Male 10-wk-old C3H/He mice were subcutaneously injected with a 0. l-ml suspension of 7 x I0^{6} syngeneic FM3A tumor cells on their left thighs. Solid tumors produced on their thighs were measured with vernier calipers and the product of three principal diameters of the tumor was designated as "tumor volume" as described previously (*17*). *A* tumor growth curve until death was obtained as the average of data from six mice. Tracer experiments were performed 10 days after transplantation.

Double-tracer Macro-autoradiography with [^{18}F]FDG and ^{3}H-Thd

A C3H/He mouse with FM3A tumors was injected with a mixture of 200 μCi (7.40 MBq) of [^{18}F]FDG and 30 μCi (1.11MBq) of [6-^{3}H] thymidine (^{3}H-Thd, Amersham Japan Ltd., Japan) and killed 1 hr later. The tumor was quickly dissected and prepared for frozen sectioning as reported previously (*18*). In brief, the trimmed tumor sample was embedded in O.C.T. compound (Miles Inc.) and frozen in isopentane cooled with liquid nitrogen. The frozen sample block was sectioned on a cryostat at −25°C. The 5 μm-thick section was mounted on a clean glass slide, air-dried and directly contacted with ARG film (MARG ^{3}H-type, Konica, Japan) for 2 hr in order to produce the [^{18}F] FDG image. Three days (about 39 half-lives of ^{18}F) after the initial autoradiography when the ^{18}F radioactivity had decayed, the same section was contacted with another film for 2 mo to produce the ^{3}H-Thd image.

Micro-autoradiography

Sixteen C3H/He male mice were transplanted subcutaneously with FM3A tumor cells. Approximately 10 days following transplantation, four mice were injected intravenously with 1 mCi (37 MBq) of [^{18}F]

Received Mar. 30, 1992; revision accepted May 28, 1992.
For reprints contact: Roko Kubota, Department of Radiology and Nuclear Medicine, Research Institute for Cancer and Tbc., Tohoku University, 4-1 Seiryo-cho, Aoba-ku, Sendai 980, Japan.

FDG, four with a mixture of 1 mCi (37 MBq) of [^{18}F]FDG and 30 μCi (1.11 MBq) of ^{3}H-Thd, and eight with 30 μCi (1.11 MBq) of ^{3}H-DG (Amersham Japan Ltd., Japan). They were killed 1 hr later. The tumors were quickly dissected and prepared for frozen sectioning as described above. Under a safety light, the 5 μm-thick sections were directly mounted on slides coated with NTB2 nuclear emulsion (Kodak) which was then cooled to −15°C. The slides were immediately deep-frozen on a dry-ice block and placed in exposure boxes cooled with dry-ice. After a 4-hr exposure for [^{18}F]FDG and a 3-wk exposure for ^{3}H-DG, they were transferred to ethanol with 5% acetic acid at −70°C and 18.5°C for 1 min each. After washing off the excess acid ethanol in water for 2 min, autoradiograms were developed in Konidol-X (Konica, Japan) for 4 min, fixed in Fuji general purpose fixer (Fuji, Japan) for 8 min and washed in gently running water for 30 min at 18.5°C. The slides were stained with hematoxylin and eosin. Nonradioactive tumor sections were subjected to the same process for chemographic control. Silver grain numbers were counted in various tumor regions under a transmitted light brightfield microscope using a micrometer. The contamination of [^{18}F]FDG microautoradiogram from simultaneously injected ^{3}H-Thd was a maximum of 0.8% during the 4 hr of exposure in a separate study, and thus was neglected.

The contiguous 5 μm-thick sections from the same frozen blocks used in the micro-autoradiographic study were mounted on clean glass slides, air-dried and directly coated with ARG films for 30 min to 1 hr in order to image [^{18}F]FDG distribution, and for 2 mo to image ^{3}H-DG distribution. The exposure duration for the [^{18}F]FDG autoradiogram was adjusted, depending on the starting time of exposure in consideration of [^{18}F]FDG decay. After the [^{18}F]FDG radioactivity had decayed, the sections labeled with simultaneously injected ^{3}H-Thd were coated with ARG films for 2 mo to image ^{3}H-Thd distribution. After this exposure, the sections were stained with hematoxylin and eosin. The micrographs were illustrated and the areas of major cell elements in each tumor were measured.

Light Microscopic Examination

The FM3A tumor tissue was fixed in a conventional 10% neutral-buffered formalin, dehydrated in graded alcohol and finally embedded in paraffin. Thin histologic sections were stained with hematoxylin and eosin using the routine staining procedure.

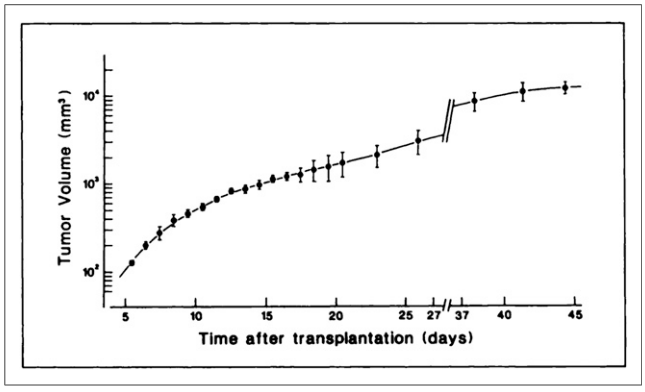

FIGURE 1. A FM3A tumor growth curve represented by daily average of every tumor measurement along the survival time of six mice. Day 0 is the day when the tumor cells were transplanted. Tumor volume of less than 100 mm^3 was technically unmeasure- able in vivo. The tracer study was performed on Day 10 when the mean tumor volume was 506 mm^3 and the mean volume doubling time was 4.4 days.

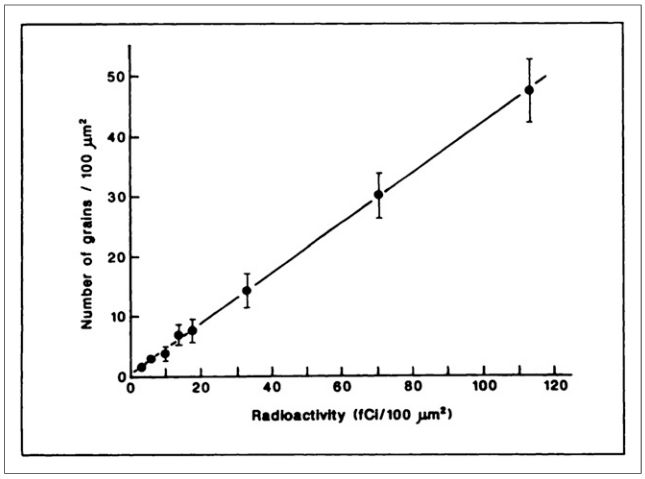

FIGURE 2. A standard curve of the relationship between silver grain numbers and ^{18}F radioactivity in micro-autoradiography. In the experimental dose range, the grain numbers were linearly related to the ^{18}F radioactivity. About 8000 grains over 1200 microgrid areas were counted for this study.

Quantitative Analysis

To determine the relationship between grain numbers and radioactivity, normal male C3H/He mice were injected intravenously with [^{18}F]FDG in different doses of 0.05 to 2.3 mCi (1.85 to 85.1 MBq) and were killed 1 min later. The 5 μm liver sections were then processed for ARG as uniform step-wise standards of radioactive sample, counterstained with eosin, and the grain numbers per unit area were counted under the transmitted light brightfield microscope using micrometer. Other 5 μm sections of the same samples were attached to thin polyethylene films, air- dried and cut into 6-mm diameter circles with a punch. The radioactivity in the punched out section was then measured with a gamma-counter. Cross calibration between the gamma counter and a well-type dose meter was performed for ^{18}F. The radioactivity per unit area of the section then was calculated and corrected for decay (*18*).

The animals used in this study were maintained in the animal care facility of our institution and the study protocol was approved by the laboratory animal care and use committee of Tohoku University.

RESULTS

Tumor Growth Curve

The tumor growth curve of subcutaneously transplanted FM3A. tumor cells on the thighs of 6 mice is shown in Figure 1. The in vivo doubling time of the tumor was about 4.4 days at the tracer experiment (10 days after transplantation). The mean survival time of the mice after transplantation was 41.8 ± 3.2 days.

Standard Curve

A standard curve relating grain numbers (grains/100 μm^2 in 5 μm-thick sections) to [^{18}F]FDG radioactivity (fCi/100 μm^2 in 5μm-sections) is shown in Figure 2. A linear relationship between the number of grains (y, grains/100 μm^2) and the corresponding [^{18}F]FDG radioactivity (x, fCi/100 μm^2) was observed ($y = 0.4171x + 0.3538$, $r = 0.9996$, $p < 0.001$). Background grain numbers (1.24 ± 0.41 grains/100 μm^2) were constant for all the experimental doses. Most of the micro-autoradiographic studies were performed within the confirmed range of linearity.

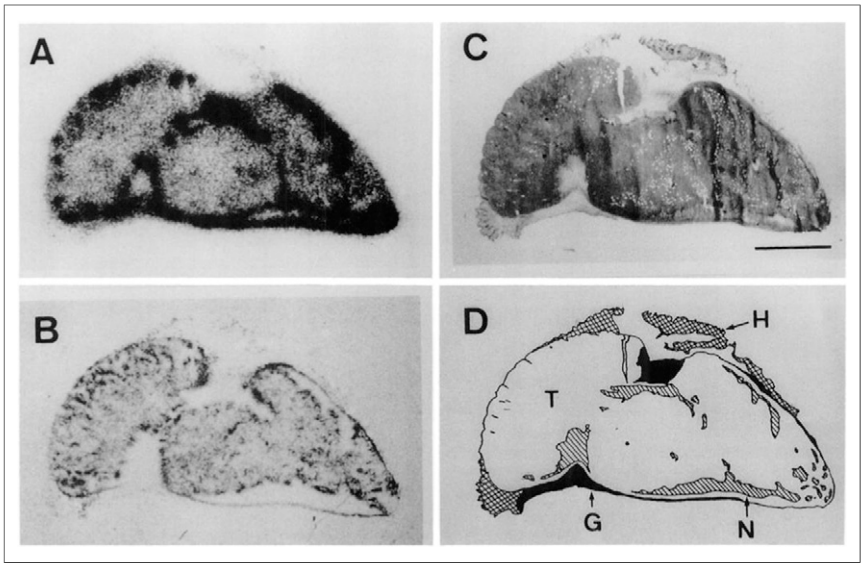

FIGURE 3. A combination of double-tracer macro-autoradiograms and microscopy. Images of [^{18}F]FDG distribution (A) and ^{3}H-Thd (B), a photomicrograph of the specimen (C) which produced the autoradiograms and the illustration of the micrograph (D). The contamination of the [^{18}F]FDG autoradiogram from ^{3}H-Thd was undetectable and that of ^{3}H-Thd autoradiogram from ^{18}F-FDG was zero. The mean 1-hr labeling index of the proliferating tumor cells by ^{3}H-Thd was 27.9% in a separate micro-ARG study. T = tumor cells; G = granulation tissue; N = necrosis; H = host normal tissue. Scale bar: 2 mm.

Double-tracer Autoradiograms with [^{18}F]FDG and ^{3}H-Thd

Figure 3 shows the autoradiograms of a FM3A tumor section l hr after the injection of a mixture of ^{18}F and ^{3}H. There were different heterogeneous distribution patterns of silver grains within the tumor which could not be explained by the resolution differences of [^{18}F]FDG and ^{3}H. The [^{18}F]FDG autoradiogram shows the high density of the tumor rim, and the accentuated dense region within the tumor corresponds to the translucent area on the ^{3}H-Thd autoradiogram. The dense area on the ^{3}H-Thd autoradiogram is consistent with the proliferating cell region by the l-hr labeling index of DNA synthesis during mitotic cycle, but the dense area on the [^{18}F]FDG autoradiogram is distributed on the whole section by glucose utilization. Both autoradiograms showed the scarce density op the normal host tissue. The differential uptake ratio of this tumor for [^{18}F]FDG was 1.368 ± 0.286 (n = 8), and the tumor-to-blood and tumor-to-muscle ratios were 10.523 and 4.035. The whole area with the grain density of ^{3}H-Thd has the grain density of [^{18}F]FDG but not vice versa, which represents the consistency and the difference between glucose utilization and the DNA synthesis in the tumor tissue. For histological confirmation, the following microautoradiography procedure was performed.

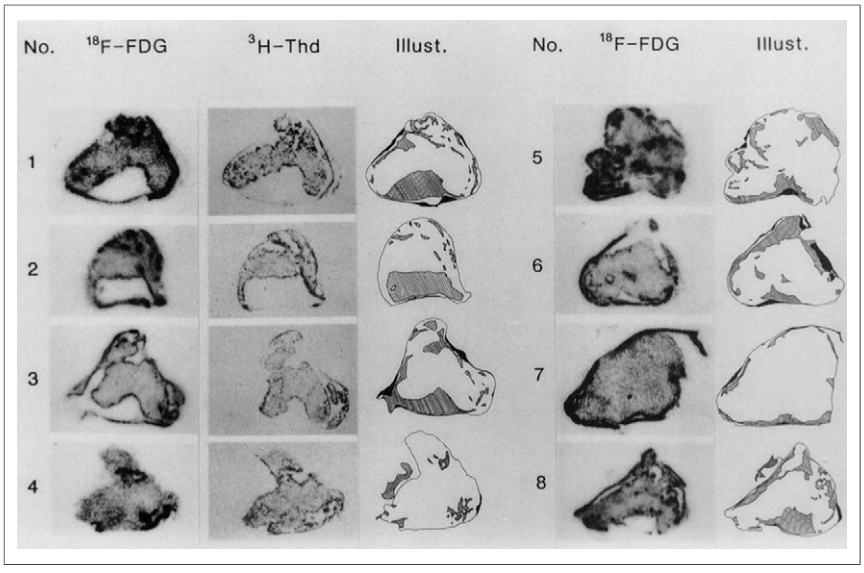

FIGURE 4. Macro-autoradiograms of [^{18}F]FDG distribution in contiguous sections for micro-autoradiography. The ^{3}H-Thd autoradiograms of four tumors (No. 1–4), which were labeled with [^{18}F]FDG and ^{3}H-Thd simultaneously, are also shown. For a simple and more informative comparison, the micrographs were added. See Figure 3 for definitions. Scale bar = 5 mm.

Macro- and Micro-autoradiography

The macro-autoradiograms of [^{18}F]FDG and ^{3}H-DG by contiguous sections for micro-autoradiography showed a similar pattern of a heterogeneous grain density in comparison with portions of the tumor mass (Figs. 4 and 5). In the autoradiograms of both [^{18}F]FDG and ^{3}H-DG, a markedly dense area surrounded the tumor itself and the central translucent area. The other dense spots were located in an area of relatively lower density. The central grain-free area was microscopically confirmed to be extensive necrotic tissue in the tumor. The autoradiograms of ^{3}H-Thd showed a different pattern from those of [^{18}F]FDG and ^{3}H-DG. The ^{3}H-Thd autoradiograms showed another heterogeneous grain density pattern in the tumor mass. The dense areas on the ^{3}H-Thd autoradiograms were observed in the tumor cell region and were not always consistent with those on the [^{18}F]FDG autoradiograms.

A combination of micro-autoradiography of [^{18}F]FDG and ^{3}H-DG and light microscopy revealed that the both tracers showed biologically the same distribution pattern, although the grain sizes and numbers were different dueto the physical nature of ^{18}F and ^{3}H. The highest grain concentration was observed on macrophages which were massively infiltrating the marginal areas surrounding extensive tumor necrosis (Fig. 6A–C). Spotty dense areas within the tumor also corresponded to areas of focal necrosis where macrophages were massively pooled (Fig. 7A–C). Whether necrosis was diffuse or focal, the grains concentrated where macrophages were present.

Young granulation tissue consisting of capillary vessels, fibroblasts and macrophages surrounded the tumor mass (Fig. 6C). The second highest grain level

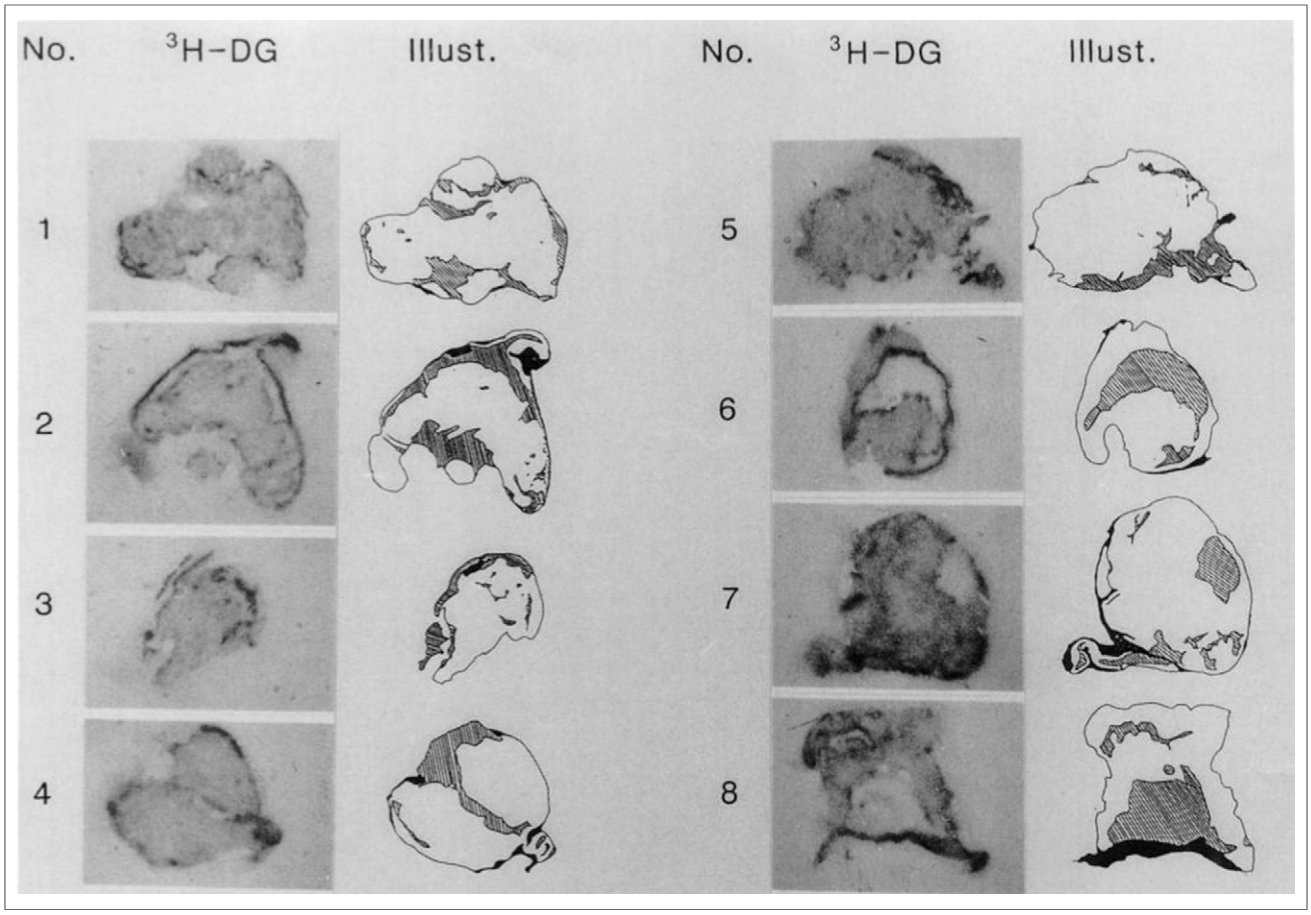

FIGURE 5. Macro-autoradiograms of ^{3}H-DG distribution in the contiguous sections for micro-autoradiography and the micrographs. See Figure 3 for definitions. The pattern of ^{3}H-DG autoradiograms was similar to that of ^{18}F-FDG autoradiograms, but was different from that of ^{3}H-Thd autoradiograms in comparison with Figure 4. Scale bar = 5 mm.

was found in this tissue. Within the granulation tissue, the grains were densely concentrated where macrophages were present (Fig. 8). The grains were also localized diffusely on viable tumor cells, but grain concentrations were relatively lower than those on the macrophages or the granulation tissue (Fig. 7).

Tables 1 and 2 show the results of grain counting for [^{18}F]FDG and ^{3}H-DG micro-autoradiographs. The tumor numbers in the tables correspond to Figures 4 and 5. The macrophage layer surrounding extensive tumor necrosis showed the highest value, which was about 3.5–3.6 times that of the tumor cells. The second highest was the young granulation tissue with capillary vessels,

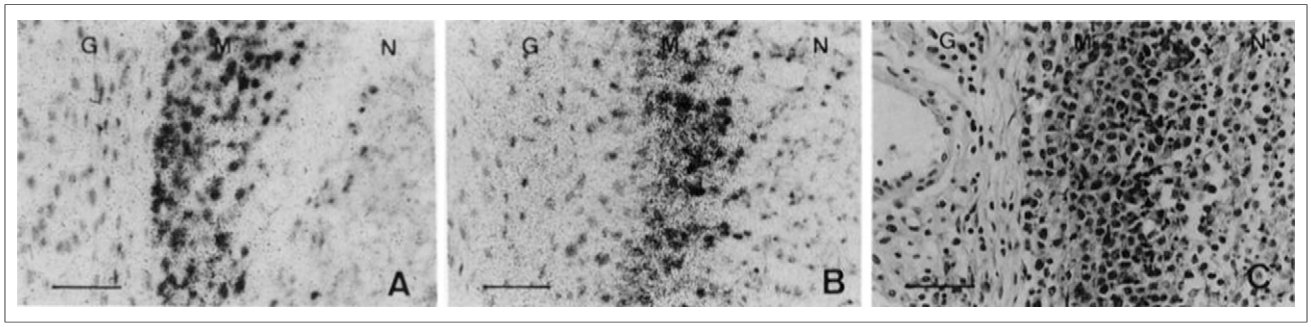

FIGURE 6. Micro-autoradiography of [^{18}F]FDG (A) and ^{3}H-DG (B). This region is the marginal areas surrounding extensive tumor necrosis near the outer surface of tumor. It consists of three layers of different cell elements: granulation tissue (G), macrophage layer (M) and necrosis (N) in order from left to right. Macrophages are observed between necrosis and granulation tissue, and the highest grain density is found in this region. Macrophages are also pooled in the necrosis and grains were distributed in this zone. Histology of the periphery of tumor tissue (C) clearly demonstrated that the macrophages, neutrophils and granulation tissue are the major components between the necrosis and the surrounding intact host tissues. Scale bar = 50 Mm.

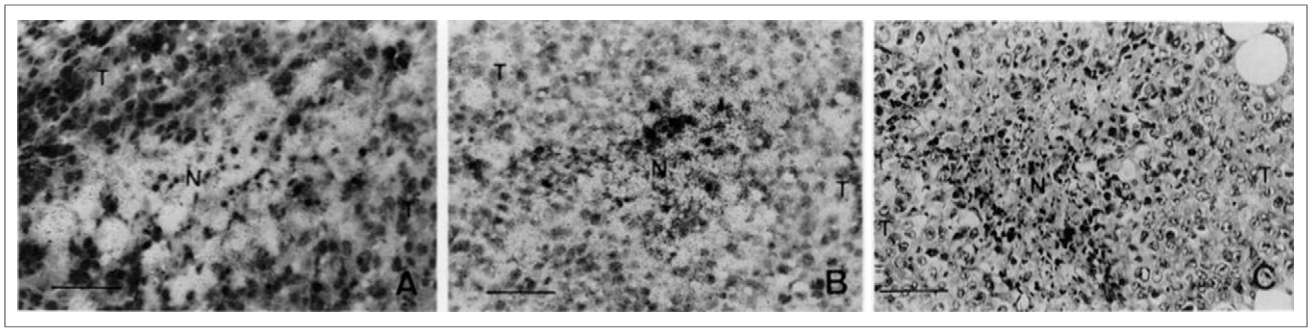

FIGURE 7. Micro-autoradiography of [^{18}F]FDG (A) and ^{3}H-DG (B). This region has a focal necrotic area with a relatively high grain density level within the tumor. Macrophages are observed among the necrotic tissue. The tumor cells around this focal necrosis showed low grain levels. Histology of the focal necrotic area (C) demonstrated that the necrosis is composed of a mixture of macrophages, neutrophils and necrotic degenerative tumor cells. The tumor cells around this area are viable. T = tumor cells and N = necrosis. Scale bar = 50 μm.

fibroblasts and macrophages surrounding the tumor mass, which showed about a 2.4–2.5 times greater value than tumor cells followed by the necrotic area with macrophages, which showed about a 2.0–2.3 times greater value than tumor cells. The necrotic area with neutrophils, which were one of major phagocytes, as well as macrophages showed the lowest value. Grain counts for both [^{18}F]FDG and the ^{3}H-DG autoradiography showed the same pattern. Semiquantitative morphometry of the micrograph is included in Tables 1 and 2. The macrophage layers were about 4.14%–4.38% and the granulation tissues were 3.55%–5.47% of the total area. The macrophage pooled areas were only a part of necrosis. It shows that about 23.85% (4.38% × 3.5 + 3.55% × 2.4) of radioactivity for [^{18}F]FDG and 28.59% (4.14% × 3.6 + 5.47% × 2.4) of that for ^{3}H-DG (no significant difference) in the whole section were derived from macrophages and granulation tissues.

Micro-autoradiographic grains were seen in all tumor tissue sections of [^{18}F]FDG injected mice, and no grain was observed in the control sections, thus ruling out the possibility of a positive chemogram.

DISCUSSION

The results can be summarized as follows: [^{18}F]FDG accumulates not only in the tumor cells but also in the inflammatory cell elements which appear in association with growth or necrosis of tumor. Accumulation of [^{18}F]FDG is relatively higher in macrophages and young granulation tissue than in the tumor cells. Macrophages are generally concentrated in the outer zones of necrosis, and granulation tissue is formed around the tumor, demarcating it from the surrounding intact host tissue. This demarcation seems to give a suitable explanation for the unique macro-autoradiographic pattern of tumor.

However, these findings do not mean that the inflammatory cells are the major source of radioactivity of [^{18}F]FDG in tumor tissue. Despite more active uptake of [^{18}F]FDG by inflammatory cells within or around the tumor, it is reasonable to consider that most of the radioactivity of [^{18}F]FDG in the whole tumor originates from viable tumor cells because they consist of the major component of the tumor mass.

Clinical studies with PET report high [^{18}F]FDG uptake in various malignant tumors, such as gliomas (*2*), hepatoma (*19*), lymphoma (*20*) and lung cancer (*21*). Minn et al. (*12*) have assessed [^{18}F]FDG accumulation in malignant tumors with PET and correlated proliferative activity of the biopsied samples with DNA flow cytometry. These authors observed a clear correlation between the proportion of the cells in S + G_2/M phases of cell cycle or the percentage of S-phase cells and [^{18}F]FDG accumulation.

Fluorine-18-FDG also accumulates in abscesses (*14,15*). This phenomenon can be explained by the active uptake of [^{18}F]FDG by phagocytes within the abscess or by granulation tissue surrounding the abscess. Interestingly, chemically produced sterile abscesses do not accumulate [^{18}F]FDG (*1*). This may be due to a different inflammatory response from that of infectious abscesses.

In the post-radiotherapy study of rat AH109A tumor model, [^{18}F]FDG accumulation by the tumor showed a slower decrease than ^{14}C-methionine and ^{3}H-thymidine uptakes (76), and the reduction patterns of [^{18}F]FDG uptake have been similar to that of ^{67}Ga-citrate, which is also considered to accumulate in phagocytes. In one PET study, the high [^{18}F]FDG uptake by colon cancer was reported to remain for a few months after radiotherapy and has been explained by the inflammatory reaction in the region (*22*).

The tumor model used in this study was subcutaneously transplanted malignant tumors. The experimental findings may not be directly applicable to human tumors because tissue response to the invading neoplasms is considered to be different in various organs, especially in the brain (*23*). However, this study suggests that one should bear in mind

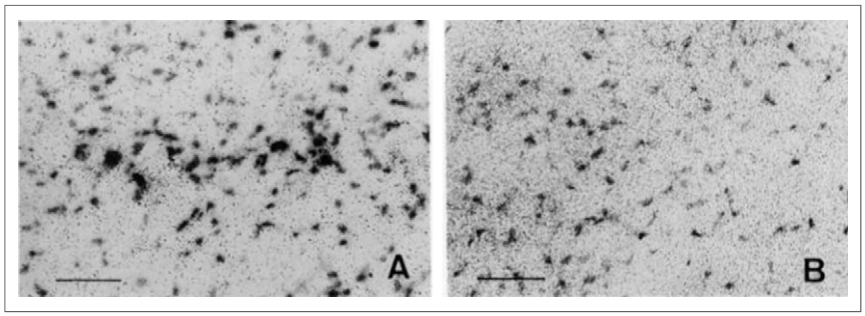

FIGURE 8. Micro-autoradiography of [^{18}F]FDG (A) and ^{3}H-DG (B). This region has young granulation tissue formed around the tumor. Macrophages were present where the grains were densely concentrated. The second highest grain density is found in this region. Scale bar = 50.

TABLE 1
Results of Microautoradiographlc Distribution of [^{18}F]FDG In FM3A

Tumor Tissues No.*	T	Number of grains / 100 μm^2					Ratios relative to Tumor Cells					Area ratio† to whole tissue (%)		
		G(fb)	G(fb,mp)	M	N(mp)	N(np)	G(fb)	G(fb,mp) M	M	N(mp)	N(np)	G	M	N
1	7.4±4.6	17.3±8.2	17.4±6.9	24.0±6.7	20.8±6.4	3.5±2.9	2.34	2.35	3.24	2.81	0.47	4.75	5.23	26.96
2	12.5±3.4	14.1±4.6	30.9±9.8	43.3±16.2	26.6±8.1	6.1±3.7	1.13	2.47	3.46	2.13	0.49	0.89	3.75	33.69
3	10.5±3.9	16.1±6.9	28.5±8.4	35.7±11.7	20.9±4.5	7.3±1.9	1.53	2.71	3.40	1.99	0.70	6.53	4.49	25.80
4	9.8±4.9	14.2±5.9	-	32.7±22.0	26.4±6.0	9.2±3.8	1.45	-	3.34	2.69	0.94	0.08	4.01	12.52
5	11.7±5.8	20.6±8.3	28.7±12.2	42.4±13.2	23.8±13.5	6.0±3.1	1.76	2.45	3.20	2.03	0.51	2.61	4.78	18.16
6	10.9±9.5	17.5±5.6	25.9±8.1	42.4±10.5	24.1±13.5	4.7±2.5	1.61	2.38	3.89	2.21	0.43	8.96	4.14	22.31
7	6.9±3.2	20.2±7.0	19.4±9.9	23.2±4.2	19.0±14.4	6.4±3.3	2.93	2.81	3.36	2.75	0.93	2.29	2.89	7.61
8	12.1±6.7	19.3±4.0	19.9±4.0	45.6±10.3	23.3±5.0	8.4±2.4	1.60	1.64	3.77	1.93	0.69	2.37	5.72	26.42
Mean	10.2±2.1	17.4±2.5‡	24.4±5.4¶‡	36.2±8.8‡	23.1±2.7‡	6.5±1.9§	1.79	2.40	3.48	2.32	0.65	3.55	4.38	21.68
S.D							0.57	0.38	0.26	0.37	0.20	3.00	0.88	8.51

T: tumor cells, G(fb): granulation tissue with fibroblasts. G(fb,mp); granulation tissue with fibroblasts and macrophages, M: macrophage layer, N(mp): macrophage pooled zone in necrosis, N(np): neutrophil pooled zone in necrosis, G: granulation tissue, N: necrosis. Each grain count data was mean ± S. D. of 8 to 12 various points in the tissue. Five to 15 microgrid areas were counted and averaged for each point.

*Tumor number corresponds to Figure 4.

†The planimetry was performed on the contiguous section used for macro-autoradiography.

‡: $p<0.001$, §: $p<0.005$ compared to tumor cells.

¶: $p<0.01$ compared to macrophages.

TABLE 2
Results of Microautoradiographic Distribution of ^{3}H-DG in FM3A

Tumor Tissues No.*	T	Number of grains / 100 μm^2					Ratios relative to Tumor Cells					Area ratio† to whole tissue (%)		
		G(fb)	G(fb,mp)	M	N(mp)	N(np)	G(fb)	G(fb,mp) M	M	N(mp)	N(np)	G	M	N
1	48.3±13.4	-	114.7±41.2	159.0±16.0	63.2±6.5	-	-	2.37	3.29	1.31	-	1.35	5.22	18.52
2	35.6±21.4	33.4±9.4	105.2±27.8	138.3±32.8	64.3±16.7	23.8±12.5	0.94	2.96	3.88	1.81	0.67	6.70	5.39	27.61
3	38.5±19.2	-	26.6±6.9	139.0±60.4	139.5±55.6	25.7± 4.6	-	0.69	3.61	3.62	0.67	3.88	6.93	21.30
4	41.3±21.8	71.0±30.6	119.4±13.6	131.5±65.5	109.7±20.2	16.1± 3.2	1.72	2.89	3.18	2.66	0.39	5.70	3.25	20.09
5	42.5±17.8	-	99.0±16.5	165.7±57.4	66.2±16.4	27.4± 5.7	-	2.33	3.90	1.56	0.64	1.76	3.49	17.97
6	35.0± 9.4	46.0±20.2	63.0±10.0	137.4±28.6	58.0±17.2	19.0± 8.3	1.31	1.80	3.93	1.66	0.54	3.53	2.73	30.40
7	41.5±17.9	70.5±22.0	122.0±32.8	143.4±26.7	73.0±12.2	30.2±16.3	1.70	2.94	3.46	1.76	0.73	9.22	3.23	15.23
8	41.7±11.5	75.2±32.7	176.7±44.3	161.4±42.7	67.7±26.2	22.4± 1.5	1.80	4.24	3.87	1.62	0.54	11.60	2.91	31.67
Mean	40.6± 4.2	59.2±18.5‡	103.3±44.2§¶	147.0±13.0**	80.2±28.8§	23.5±4.9**	1.50	2.53	3.64	2.00	0.60	5.47	4.14	22.85
S.D.							0.36	1.03	0.30	0.76	0.12	3.59	1.51	6.19

T: tumor cells, G(fb): granulation tissue with fibroblasts, G(fb,mp): granulation tissue with fibroblasts and macrophages, M: macrophage layer, N(mp): macrophage pooled zone in necrosis, N(np): neutrophil pooled zone in necrosis, G: granulation tissue, N: necrosis. Each grain count data was mean ± S.D. of 8 to 12 various points in the tissue. Three to 7 microgrid areas were counted and averaged for each point.

*Tumor number corresponds to Figure 5.

†The planimetry was performed on the contiguous section used for macro-autoradiography.

‡: $p<50.02$, §: $p<0.002$, **: $p<0.001$ compared to tumor cells.

¶: $p<0.02$ compared to macrophages.

that higher tumor uptake may reflect not only tumor cell viability and proliferation but also the contribution of secondary inflammatory reaction elements. Further micro-autoradiographic studies with [^{18}F]FDG will be of help in understanding PET's role in clinical problems.

ACKNOWLEDGMENTS

The authors are grateful to Dr. Prantika Som, Brookhaven National Laboratory, Upton, NY, for advice; to the staffs of the Cyclotron and Radioisotope Center, Tohoku University, for their cooperation; and to Mr. Y. Sugawara for photography. This work was supported by a grant-in-aid for scientific research (03152018, 03454277 and 04557047) from the Ministry of Education, Science and Culture, Japan.

REFERENCES

1. Som P, Atkins HL, Bandoypadhyay D, et al. A fluorinated glucose analog, 2-fluoro-2-deoxy-D-glucose (F-18): non-toxic tracer for rapid tumor detection. *J Nucl Med* 1980;21:670–675.
2. Larson SM, Weiden PL, Grunbaum Z, et al. Positron imaging feasibility studies. II. Characteristics of 2-deoxyglucose uptake in rodent and canine neoplasms: concise communication. *J Nucl Med* 1981;22:875–879.
3. Di Chiro G, DeLaPaz RL, Brooks RA, et al. Glucose utilization of cerebral gliomas measured by [^{18}F]-fluoro-deoxyglucose and positron emission tomography. *Neurology* 1982;32:1323–1329.
4. Yonekura Y, Benua RS, Brill AB, et al. Increased accumulation of 2- deoxy-2-(^{18}F)fluoro-D-glucose in liver metastases from colon carcinoma. *J Nucl Med* 1982;23:1133–1137.
5. MacKeehan WL. Glycolysis, glutaminolysis and cell proliferation. *Cell Biol Int Rep* 1982;6:635–650.
6. Weber G, Morris HP, Love WC, Ashmore J. Comparative biochemistry of hepatomas. II. Isotope studies of carbohydrate metabolism in Morris hepatoma 5123. *Cancer Res* 1961;21:1406–1411.
7. Weber G. Enzymology of cancer cells. *N Engl J Med* 1977;296:541–551.
8. Monakhov NK, Neistadt EL, Shavlovski MM, Shvartsman AL, Neiufakh SA. Physicochemical properties and isoenzyme composition of hexokinase from normal and malignant human tissues. *J Natl Cancer Inst* 1978;61: 27–34.
9. Renner ED, Plagemann PGW, Bemlohr RW. Permeation of glucose by simple and facilitated diffusion by Novikoff rat hepatoma cells in suspension culture and its relationship to glucose metabolism. *J Biol Chem* 1972; 247:5765–5776.
10. Kubota K, Matsuzawa T, Fujiwara T, et al. Differential diagnosis of lung tumor with positron emission tomography: a prospective study. *J Nucl Med* 1990;31:1927–1933.
11. Di Chiro G. Positron emission tomography using [^{18}F]fluorodeoxyglucose in brain tumors, a powerful diagnostic and prognostic tool. *Invest Radiol* 1987;22:360–371.
12. Minn H, Joensuu H, Ahonen A, KJemi P. Fluorodeoxyglucose imaging: a method to assess the proliferative activity of human cancer in vivo. Comparison with DNA flow cytometry in head and neck tumors. *Cancer* 1988; 61:1776–1781.
13. Paul R, Johansson R, Kellokumpu-Lehtinen P-L, Soderstrom K-O, Kangas L. Tumor localization with ^{18}F-2-fluoro-2-deoxy-D-glucose: comparative autoradiography, glucose 6-phosphatase histochemistry, and histology of renally implanted sarcoma of the rat. *Res Exp Med* 1985;185:87–94.
14. Tahara T, Ichiya Y, Kuwabara Y, et al. High [^{18}F]fluorodeoxyglucose uptake in abdominal abscesses: a PET study. *J Comput Assist Tomogr* 1989:13:829–831.
15. Sasaki M, Ichiya Y, Kuwabara Y, et al. Ringlike uptake of [^{18}F]FDG in brain abscess: a PET study. *J Comput Assist Tomogr* 1990;14:486–487.
16. Kubota K, Ishiwata K, Kubota R, et al. Tracer feasibility for monitoring of tumor radiotherapy: a quadruple-tracer study with ^{18}F-FDG or ^{18}F-FdUrd, ^{14}C-Met, ^{3}H-Thd and ^{67}Ga. *J Nucl Med* 1991;32:2118–2123.
17. Kubota K, Kubota R, Matsuzawa T. Dose-responsive growth inhibition by glucocorticoid and its receptors in mouse teratocarcinoma OTT6050 in vivo. *Cancer Res* 1983;43:787–793.
18. Yamada S, Kubota R, Kubota K, Ishiwata K, Ido T. Localization of [^{18}F] fluorodeoxyglucose in mouse brain neurons with micro-autoradiography. *Neurosci Letts* 1990; 120:191 -193.
19. Paul R, Ahonen A, Nordman E. Imaging of hepatoma with [^{18}F] fluorodeoxyglucose. *Lancet* 1985;1:50–51.
20. Paul R. Comparison of fluorine-18-2-fluorodeoxyglucose and gallium-67 citrate imaging for detection of lymphoma. *J Nucl Med* 1987;28:288–292.
21. Nolop KB, Rhodes CG, Brudin LH, et al. Glucose utilization in vivo by human pulmonary neoplasms. *Cancer* 1987;60:2682–2689.
22. Haberkom U, Strauss LG, Dimitrakopoulou A, et al. PET studies of fluorodeoxyglucose metabolism in patients with recurrent colorectal tumors receiving radiotherapy. *J Nucl Med* 1991;32:1485–1490.
23. Blasberg RG, Shinohara M, Shapiro WR, Patlak CS, Pettigrew KD, Fenstermacher JD. Apparent glucose utilization in Walker 256 metastatic brain tumors. *J Neurooncol* 1986;4:5–16.